Research Article Vol. 12, No. 8 / August 2024 / Photonics Research 1619

PHOTONICS Research

Frequency stabilization of C-band semiconductor lasers through a SiN photonic integrated circuit

Alessandro Brugnoni,[1,2,*] Ali Emre Kaplan,[1,2] Valerio Vitali,[1,2] Kyle Bottrill,[2] Michele Re,[3] Periklis Petropoulos,[2] Cosimo Lacava,[1] and Ilaria Cristiani[1]

[1]Photonics Group, Department of Electrical, Computer and Biomedical Engineering, University of Pavia, Pavia 27100, Italy
[2]Optoelectronics Research Centre, University of Southampton, Southampton SO17 1BJ, UK
[3]Huawei Technologies Italia S.r.l, Centro direzionale Milano, Segrate 20054, Italy
*Corresponding author: alessandro.brugnoni01@universitadipavia.it

Received 21 December 2023; revised 26 March 2024; accepted 23 April 2024; posted 24 April 2024 (Doc. ID 516588); published 15 July 2024

Integrated semiconductor lasers represent essential building blocks for integrated optical components and circuits and their stability in frequency is fundamental for the development of numerous frontier applications and engineering tasks. When dense optical circuits are considered, the stability of integrated laser sources can be impaired by the thermal cross-talk generated by the action of neighboring components, leading to a deterioration of the long-term system performance (on the scale of seconds). In this work we show the design and the experimental characterization of a silicon nitride photonic integrated circuit (PIC) that is able to frequency stabilize 16 semiconductor lasers, simultaneously. A stabilized 50 GHz-spaced two-channel system is demonstrated through the detection of the related beating note and the stability of the resulting waveform is characterized via the use of artificially induced thermal cross-talk stimuli.

https://doi.org/10.1364/PRJ.516588

1. INTRODUCTION

Silicon photonics and related integrated photonic platforms have shown to be fundamental in resolving technical challenges in a variety of fields, optical communications, sensing, biology, and food quality monitoring, to name a few of them [1–5]. As a consequence, the great interest of the industry in providing increasingly reliable and high-throughput systems for such applications, along with the need to scale the technology [6,7], led to the implementation of new silicon-photonics-based structures. For instance, one enabling device for future applications in communications is represented by tunable sources of THz signals (0.05–1 THz) [8–11]. A possible path to the realization of such a component is the use of highly stable, frequency-locked, semiconductor lasers, arranged in a heterodyne beating note scheme [12–15]. However, the emission frequency of semiconductor sources is very sensitive to local temperature variations and thermal fluctuations that could arise from environmental conditions, diffusion currents, or fabrication errors [16,17]. Additionally, the execution of complex functions requires the integration of an increasing number of components and devices on the same chip, possibly leading to the generation of thermal cross-talk between closely spaced devices. This could be the case of multiple lasers integrated in the same array [18,19] or reconfigurable photonic networks that widely employ thermal actuators as the tuning mechanism [20–22]. A frequency drift of the light source could result in a strong performance impairment, for example, in super-channel transmission schemes this might lead to an overlap of sub-carriers, thus affecting the complexity of the digital signal processing (DSP) steps and/or the data rate of the transmitting signals [23,24]. Thermal cross-talk-related effects in densely packed circuits can be mitigated via different approaches; one of the proposed solutions relies on the use of insulation trenches [25–27]; however, these structures are only beneficial when utilized to thermally isolate relatively large photonic devices, such as Mach-Zehnder interferometers, and are therefore not suitable for use with, for example, microring resonators (MRRs) [28,29]. In contrast, feedback-based solutions rely on specific algorithms that are able to correct any thermal drift that might arise in the circuit; they do not need any additional fabrication steps and are independent of the circuit topology [29,30].

In this paper we describe the design and characterization of a silicon nitride (SiN) photonic integrated circuit (PIC) with the ability to independently manage multiple C-band semiconductor lasers and retain their frequency stability within an accuracy of approximately 10 MHz, even with a laser subjected to an artificial thermal stimulus (test ramp of −125 MHz/hour), while a beating note of 50 GHz is considered between this laser and an unperturbed one. This result is achieved by locking the frequency of each laser to the resonance(s) of a high-Q ring resonator fabricated onto the SiN PIC, acting as a wavelength reference and frequency meter. Specifically, as shown in

Section 2, the PIC is able to retrieve a signal error related to the frequency drift of each light source and provide a dedicated electrical feedback signal to each laser tuning circuitry. The correction time is below 200 ms and is only limited by the thermo-optic response of the driving circuit of the lasers.

The paper is organized as follows. We first discuss the laser frequency stabilization algorithm that we implemented in a closed-loop configuration followed by a section describing the design and the characterization of the SiN PIC. Here we explain the criteria we followed in the design and show the experimental implementation of the algorithm discussed in the previous section. The last part is devoted to the use of the SiN PIC to stabilize and frequency-lock two narrow-linewidth semiconductor lasers, utilized to generate a 50 GHz beating note. The stability of the generated frequency tone is investigated through the use of an artificial thermal stimulus, applied to the semiconductor lasers, mimicking the thermal noise that might be naturally present in a complex integrated circuit.

Different frequency stabilization methods can be already found in the literature [31,32]. Our system offers two main advantages with respect to the other approaches: (i) it can be employed with any integrated laser technology (with the availability of a feedback line access) and (ii) supports simultaneously the stabilization of 16 units, thus making the system suitable for large scale photonic circuit integration. To the best of our knowledge, our results demonstrate, for the first time, the capability to perform precise frequency locking of multiple sources exploiting a single PIC with a 5 mm × 10 mm footprint and an enhanced thermal stability, providing an unprecedented tool for the development of Tb/s transmission links based on the generation of THz beat notes.

2. ALGORITHM WORKING PRINCIPLE

The basic working principle of the proposed stabilization scheme is based on a negative feedback loop, as schematically shown in Fig. 1(a). Specifically, the emission frequency of each laser source is aligned to the inflection point of a resonance of a high-Q-factor periodic transmission filter [FL—frequency locker; see Fig. 1(b)]. In this way, any frequency drift Δf that might occur on the laser line under consideration is translated into a power variation ΔP at the output [PD_1 in Fig. 1(a)]; the power fluctuation is photo-detected via on-chip photodetectors and sent to an external micro-controller coded in Python that instructs the emitting device with an appropriate feedback signal that is proportional to the recorded power variation. In order to eliminate any ambiguity that might originate from power fluctuations of the source itself, the laser signals are

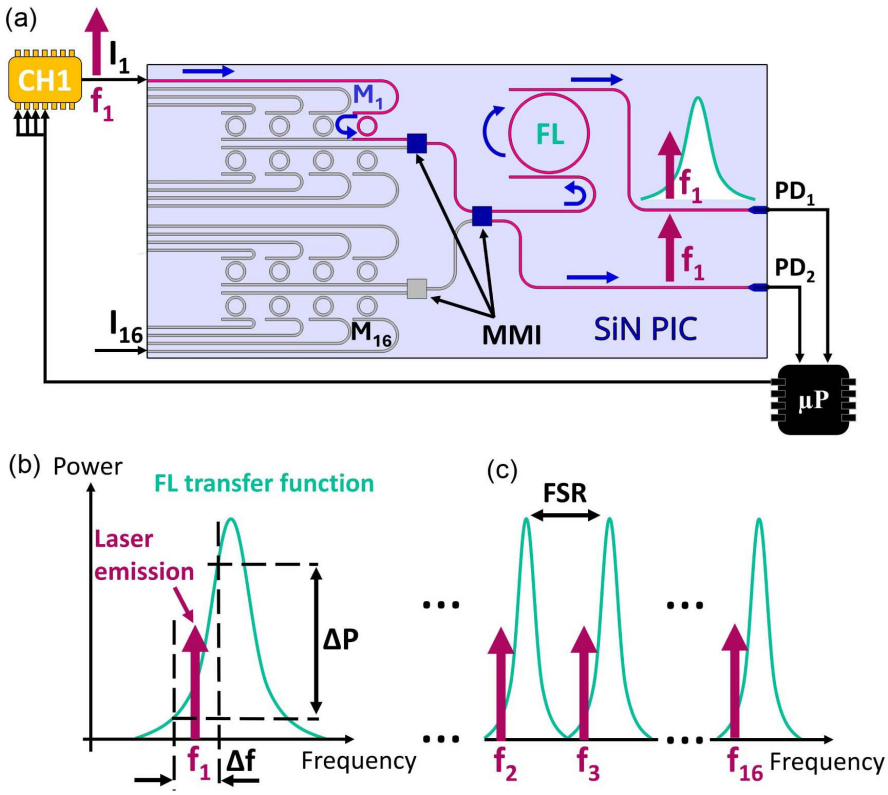

Fig. 1. (a) Laser frequency stabilization architecture based on a packaged integrated SiN PIC and a negative feedback configuration. The different laser sources (e.g., CH1 at frequency f_1) are fed at the input of the PIC and coupled via MMIs to the frequency locker (FL) ring. Two photodiodes, at the output PD_1 and PD_2, detect the power variations related to each source. A micro-processor uses these variations to stabilize each laser frequency. The coding of intensity optical modulators (M_1 to M_{16}) guarantees the multiple detection and stabilization of the input sources; CH1, channel one; MMI, multi-mode interferometer; µP, micro-processor. (b) Laser frequency drifts (Δf) detection based on the generation of an error signal (ΔP) given by the laser emission frequency with respect to the FL resonance. (c) Different laser sources can be locked along different FL resonances whose spacing is defined by the FL free spectral range (FSR). The current implementation allows the connection of 16 input sources.

also coupled to another output (PD_2) that does not involve the FL. By calculating the ratio between the electrical signals at the two outputs, the frequency fluctuations can be isolated, discarding any laser power fluctuation that might also take place during the operation.

Additionally, a stable frequency grid can then be obtained by locking multiple sources to the resonances of the same on-chip FL [as shown in Fig. 1(c)]. The proposed schematic is equipped with 16 inputs that allow to manage up to an equivalent number of sources. In order to provide dedicated feedback to each frequency, the radiation of each input laser is modulated by operating 16 MRRs as optical intensity modulators (M_1 to M_{16}) that assign a code division multiple access (CDMA) [33] sequence to each input. As a consequence, the feedback signal related to each laser can be recovered by a decoding step that is carried out by the external micro-controller.

3. PIC DEVELOPMENT AND CHARACTERIZATION

We selected a low-loss SiN platform for the implementation of the photonic circuit described in the previous section. This technology allowed to realize (i) 10^3-Q level ring resonators [34,35] with low loss and high stability with respect to thermal fluctuations, (ii) free spectral range (FSR) values on the order of 0.05 to 0.25 THz with no variations over the C-band (i.e., a low-dispersion platform [36]), and (iii) the ability to realize kHz-rate optical modulators with minimal optical loss and low electrical power consumption.

Specifically, we selected the Multi-Project Wafer platform provided by Ligentec that ensures waveguides with low loss ($\alpha \approx 0.2$ dB/cm) and zero dispersion at a wavelength of $\lambda = 1550$ nm. This can be achieved using waveguides with a thickness of 800 nm [see Fig. 2(a)]. The final layout is shown in Fig. 2(b). The schematic includes 16 input channels, each of them connected to a thermo-optic modulator (M_1 to M_{16}) with 1 kHz bandwidth. In order to minimize the PIC footprint, a common drop port was shared every four modulators [as shown in the previous Fig. 1(a)]. The number of modulators in each shared bus waveguide was chosen in such a way as to allow the independent modulation of each laser source through the FL. This is obtained by the following relationship between the FSR and the 3 dB bandwidth (BW) of the i-th modulator: $\mathrm{FSR}_i > \mathrm{BW}_i \times N$, $i = 1, 2, 3, \ldots$, where N is the number of modulators that share a common bus waveguide. In our case each modulator was designed using a gap of 350 nm and a bending radius with 90 μm of nominal value (slightly different from one to another in order to obtain distinct resonances over the C-band) as depicted in Table 1.

The expected FSR and 3 dB bandwidth for the i-th modulator were ~250 GHz and ~10 GHz, respectively, widely satisfying the aforementioned relationship. A total of four bus waveguides were required to retrieve the information related to 16 possible input laser sources. Two 2 × 1 multi-mode interferometers (MMIs) were used to couple two pairs of waveguides [refer to Fig. 1(a)]. An additional 2 × 2 MMI was necessary to merge the two remaining waveguides and split them into two outputs. One branch is directly read at the output [corresponding to PD_2 in Fig. 1(a)], while the other is first

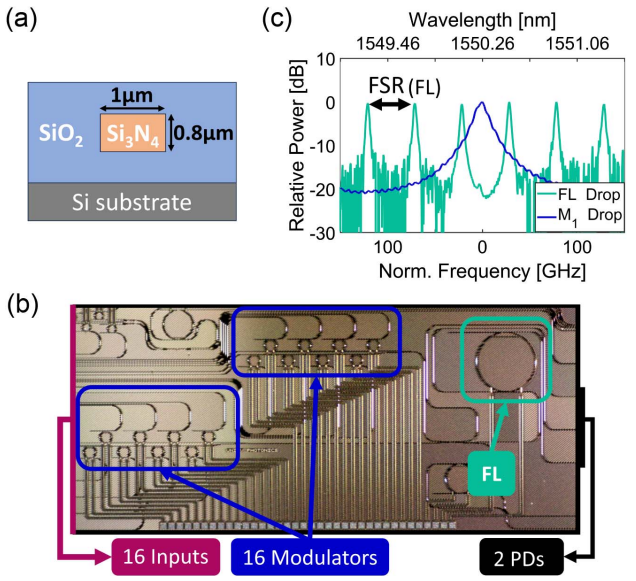

Fig. 2. (a) Cross section of the Si_3N_4 waveguide constituting the PIC layout. The waveguide dimensions are set to obtain zero-dispersion operation along the C-band. (b) Main building blocks of the frequency stabilizer PIC. The fabricated chip is composed of 16 inputs, 16 thermo-optic modulators, and a frequency locker (FL) shared among all the input paths and two outputs. The latter are equipped with on-chip photo-detectors. (c) Static characterization of the FL and first modulator drop port transfer function. The frequency is normalized with respect to 193.38 THz and the optical power to 0 dB. The FL FSR is set to be 50 GHz; FSR, free spectral range.

coupled to the FL and its output is sent to PD_1. Both the input and the output ports were provided with inverted-taper-based fiber coupling devices. Before proceeding to the final packaging, the chip was first characterized using a standard input/output fiber experimental set-up aiming at extracting the transfer functions of the fabricated modulators and devices. Coupling loss and waveguide propagation loss were estimated to be 1.7 dB/facet and 0.2 dB/cm, respectively. In Fig. 2(c) we report the experimental transfer function extracted for one representative modulator device (M_1) depicted in blue, while in green we report the transfer function of the FL device, recorded at the PD_1 output. The results showed very good agreement with the design target (see Table 1).

Thermal actuators were integrated both on the modulators and on the FL, so that the transfer function of every device

Table 1. Designed and Measured Parameters of the Generic Modulator M_i and of the FL in the PIC[a]

	Designed				Measured	
Device	Radius [μm]	Gap [nm]	FSR [GHz]	3 dB BW [GHz]	FSR [GHz]	3 dB BW [GHz]
M_i	90	350	250	10	~250	~15
FL	450	550	50	2	~50	~3.7

[a]The gap is defined as the spacing between the straight waveguide and the ring-shaped one; FSR, free spectral range; 3 dB BW, 3 dB bandwidth.

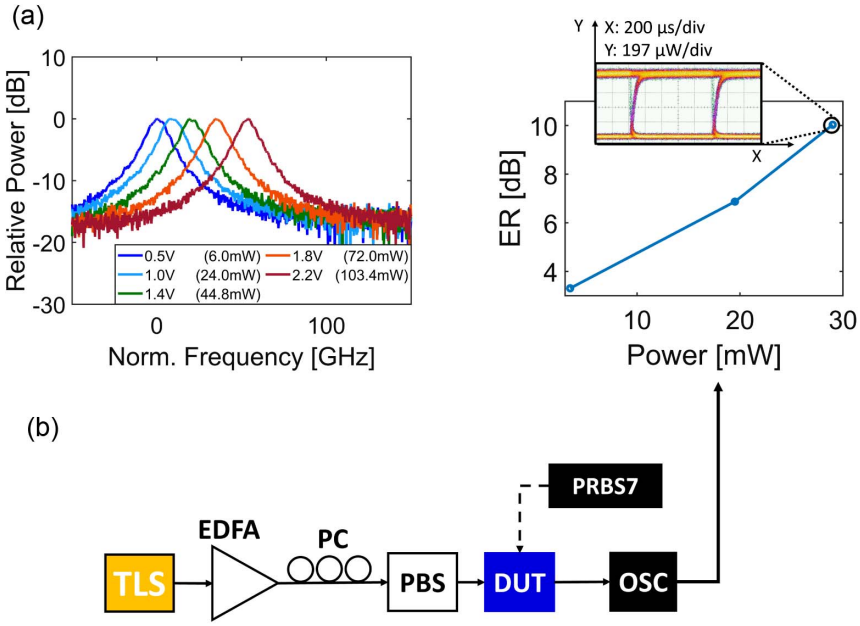

Fig. 3. (a) Thermal tuning of the M_1 modulator. The frequency is normalized with respect to 193.38 THz and the optical power to 0 dB. (b) Experimental set-up for the eye diagram analysis. The device under test (M_1 modulator) was modulated with a 1 kHz PRBS7 on–off keying (OOK) modulation. The maximum extinction ratio (ER) of 10 dB was read on the oscilloscope for an applied power of ~30 mW; PRBS7, seven bits pseudo random binary sequence; TLS, tunable laser source; EDFA, erbium-doped fiber amplifier; PC, polarization controller; PBS, polarization beam splitter; DUT, device under test; OSC, oscilloscope.

could be accurately tuned along the C-band. A measured thermal tuning efficiency of almost 4.4 pm/mW was retrieved for the generic modulator [Fig. 3(a)]. Dynamic characterization was also performed at a frequency of 1 kbit/s using an on–off keying (OOK) test signal [set-up and measurements depicted in Fig. 3(b)]. Results showed that an extinction ratio (ER) of 10 dB and an open eye diagram could be obtained by applying an electrical power of 30 mW.

The PIC was subsequently fully packaged [see Fig. 4(a)] and integrated with two edge-illuminated InGaAs photo-detectors (bandwidth of 1.5 GHz) aligned at the PD_1 and PD_2 outputs, while polarization maintaining (PM) single mode fibers were aligned and packaged at the input ports, as shown in Fig. 4(b). Transimpedance amplifiers and electrical connections to the heaters were provided by an on-chip analog front-end aimed to detect the photocurrents of the reversely biased pin junctions and thermally tune the MRRs (modulators and FL), respectively. The chip was finally mounted on a temperature-controlled case.

4. DEMONSTRATION OF PIC OPERATION

The PIC was tested in three different experiments. The first test was carried out in order to verify that the outputs of PD_1 and PD_2 were correctly monitoring the frequency fluctuations of a test laser. In the second set of experiments, we tested the PIC and the developed correction algorithm with a single narrow-band semiconductor laser. The final test allowed to test the system when two lasers were simultaneously fed into the chip. In this case we monitored the beat signal produced by their interference, to test the ability of the system to stabilize a beat note at 0.05 THz.

In Fig. 5(a) we show the experimental set-up we utilized to test the capability of the system to monitor the frequency

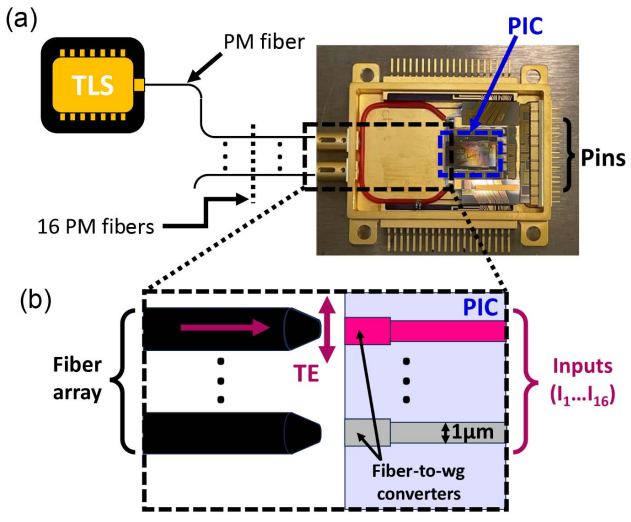

Fig. 4. Alignment set-up between an external laser and the SiN PIC. (a) A linearly polarized light is emitted by a tunable laser source (TLS). Its light is coupled through a polarization-maintaining (PM) fiber to one input of the PIC (blue square). The circuit was fully packaged providing a thermo-electric cooler (TEC) at the bottom and on-chip photo-detectors at the output. The latter, along with the modulator heaters, were accessed by external pins. (b) Alignment of 16 fibers was guaranteed by butt-coupling the arrayed fibers with the input waveguides of the PIC in order to excite the TE mode.

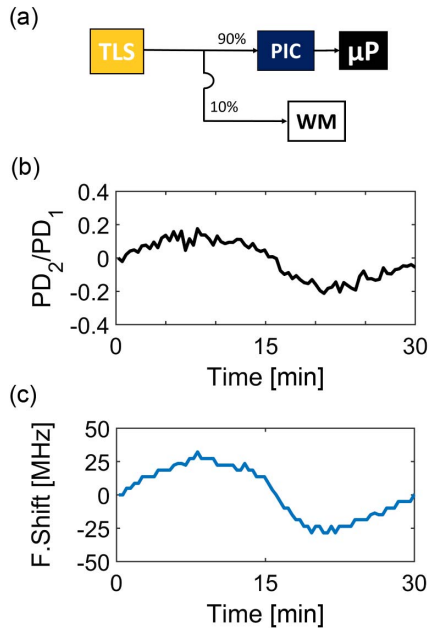

Fig. 5. (a) A Keysight 8168F commercial laser was fed to one input of the PIC and its frequency was evaluated using a wavelength meter over a 30 min time window. (b) The trend detected at the µP side as the ratio between the outputs of PD_2 and PD_1 (normalized to the initial value) perfectly matched (c) the shift recorded at the wavelength meter side. TLS, tunable laser source; PIC, photonic integrated circuit; µP, micro-processor; WM, wavelength meter.

fluctuations of a laser under test. We sent a commercial Keysight 8168F laser to our chip and we used the system to record the ratio between the PD_2 and PD_1 ports, as depicted in Fig. 5(b). The absolute frequency of the laser under test was independently monitored via a commercial Yokogawa AQ6151 wavelength meter [see Fig. 5(c)]. The results revealed that the ratio correctly traced the frequency variations of the laser over a 30 min time span. As expected, no variations were recorded at the ratio when the output power of the laser was manually varied.

In the second set of experiments, we replaced the optical source with an external cavity tunable laser prototyped by Huawei. This C-band operating semiconductor laser featured a linewidth of about 10 kHz and an output power of a few tens of mW (see Fig. 6). First, the frequency stability of the laser under test was evaluated in free-running operation as shown in Fig. 6(a). Then the feedback of the system was activated [see Fig. 6(b)] with the aim of stabilizing the thermal drift of the light source. The results of the tests are shown in a histogram where the frequency was acquired every 10 s. The tolerable threshold for the single laser was set to an arbitrary absolute value of 50 MHz in order to point out the operation limits of the algorithm. When the feedback was deactivated, the frequency was continuously drifting over a 2 h time window, crossing the 50 MHz limit after 50 min acquisition. In this case the event counts were evenly distributed over the different frequency values. Due to the minimal resolution of the wavelength meter, a slight spreading was applied to each sample

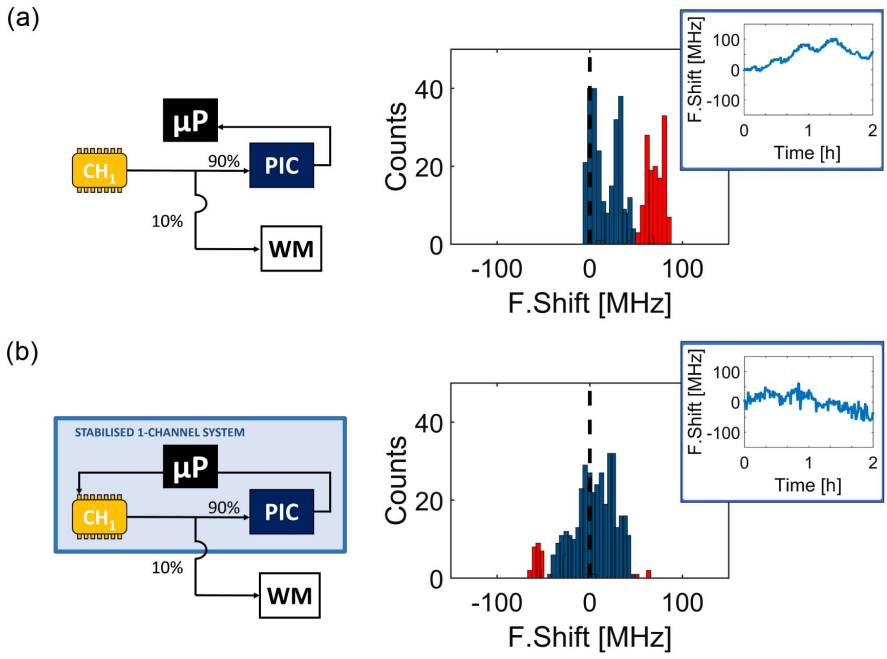

Fig. 6. Evaluation of the thermal frequency drift of a Huawei semiconductor laser when the negative feedback is (a) off or (b) on. The related schematics are shown on the left side. On the right side, the respective histograms show blue bars when the frequencies are retained within an absolute value of 50 MHz, while red bars when this limit is crossed. When the algorithm was off (a), the counts of frequency values were evenly distributed over the histogram, showing a continuous drift of the channel (red bar count is often above 10). The histogram resembled a quasi-Gaussian noise when the connection was established [(b), right side] with a few MHz average value (red bar count is below 10). The insets on the right corner depict the related frequency drift over time.

in order to make the distribution easily visible. When the feedback system was enabled, the frequency variations were kept within an accuracy of a few MHz over the same time period, showing few counts outside of the permitted frequency window (Gaussian-like distribution).

The frequency locking of two laser lines (CH_1 and CH_2) was then demonstrated by tuning the emission of the two lasers in correspondence with the inflection points of two subsequent resonances of the FL that are 50 GHz apart. The thermo-optic modulators assigned a CDMA sequence (with a 1 kHz bit rate) to each laser under use; thus the frequency variations related to each laser could be independently detected at the photodiodes.

A schematic of the set-up that was employed is shown in Fig. 7. A fraction of the power of each laser was tapped and coupled through a set of 3 dB optical fiber couplers. The extracted power was amplified via an EDFA and sent to a high-speed photodiode that allowed the detection of the 50 GHz tone. The algorithm effectiveness and stability were monitored by mixing the 50 GHz tone with a signal frequency tone (f_{WG}) generated by a commercial radio frequency synthesizer (Anritsu MG3695B) operating at 46 GHz. The down-converted low-frequency (~4 GHz) signal at the output of the mixer was read by an RF spectrum analyzer (RFSA, Agilent E4446A, resolution bandwidth of 3 MHz).

The system was tested with three different thermal stimuli, going from the slowest to the fastest one, that were applied to one of the two lasers under consideration. The first stimulus was a slow ramp (2 h duration) that was calibrated to induce

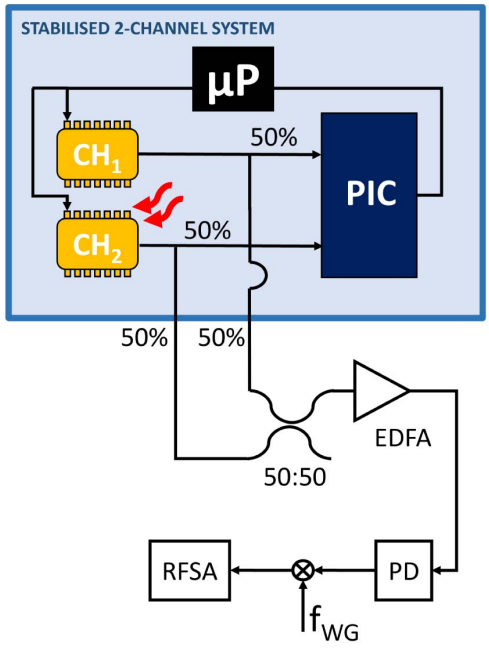

Fig. 7. Two 50 GHz-spaced lasers (CH_1 and CH_2) were stabilized in frequency through the shown set-up (blue box). The power of the two lasers was coupled via 3 dB couplers, amplified (EDFA), and detected by a fast photodiode (PD) to retrieve the 50 GHz note, generated by the separation of the lasers frequencies. The high-frequency content was then down-converted using an external frequency (f_{WG}) and the base-band signal was read by an RF spectrum analyzer. f_{WG}, waveform generator frequency; RFSA, RF spectrum analyzer; PD, photodiode; EDFA, erbium-doped fiber amplifier.

a −250 MHz frequency drift to one of the lasers under consideration. As shown in Fig. 8(a), red line, when the algorithm was turned off and no feedback signal was fed to the laser, the beating note showed a frequency drift with respect to the nominal value of −250 MHz, following exactly the thermal stimulus artificially applied to the laser. When the feedback was turned on the system was able to keep the beat frequency constant at 50 GHz (to within ±10 MHz) as shown in Fig. 8(a), blue line. Similarly, a second test was utilized to test the system response against the application of a co-sinusoidal stimulus (induced peak to peak change in the beating note frequency of 500 MHz), as shown in Fig. 8(b). Also in this case the system responded to the externally induced noise by stabilizing the system around the designated 50 GHz beating note frequency. As a final test, we applied a 50 s square wave stimulus to the system in order to excite a −500 MHz change in the beating note, as shown in Fig. 8(c), red line. As expected, the algorithm was able to correct the steep change. Spurious peaks related to the slow thermo-optic transient of the laser tuning (~600 ms) and the minimal time response of the algorithm (200 ms) were still observed during the correction (blue curve) limiting the fast response of the system.

5. CONCLUSIONS

The design and experimental demonstration of an electrical closed-loop configuration based on a packaged integrated silicon nitride circuit that allows the stabilization of multiple laser sources placed on a 50 GHz-spaced grid have been presented. The enabling building block consists of a high-Q ring resonator, whose resonance is used as a reference to lock the laser frequency by thermal tuning of its position. The FL has been designed to provide a free spectral range that ensures a channel spacing of 50 GHz between adjacent channels. The system was tested with two 50 GHz-spaced semiconductor lasers that were fed to the SiN PIC and different thermal stimuli were applied to one of them, so that it was possible to mimic the thermal drift of the laser frequency in a crowded chip. The experimental results were obtained by the heterodyne detection of the generated 50 GHz beat note, showing the adaptive response of the circuit both to steep and slowly varying changes. A −125 MHz/hour ramp was promptly counteracted by the negative feedback, showing the possibility of mitigating the effect of thermal cross-talk produced by the neighboring components in a densely integrated chip (~few MHz/s expected variation).

Thanks to the PIC design, the system allows to lock 16 laser sources, and might be used to generate a super-channel on a dense WDM scheme (up to 800 GHz with the current implementation). This architecture can find also application in heterodyne generation of sub THz or THz signals, where the emission frequency is set by the separation between two laser sources. The algorithm was demonstrated for a 50 GHz tone generation, but in principle, a multiple of this frequency can be generated and stabilized by the algorithm. In conclusion, the developed integrated platform together with the locking algorithm has been demonstrated as a simple and powerful method to mitigate thermal cross-talk in a crowded chip, offering potential benefits to the implementation of stable THz-frequency sources and the generation of superchannels

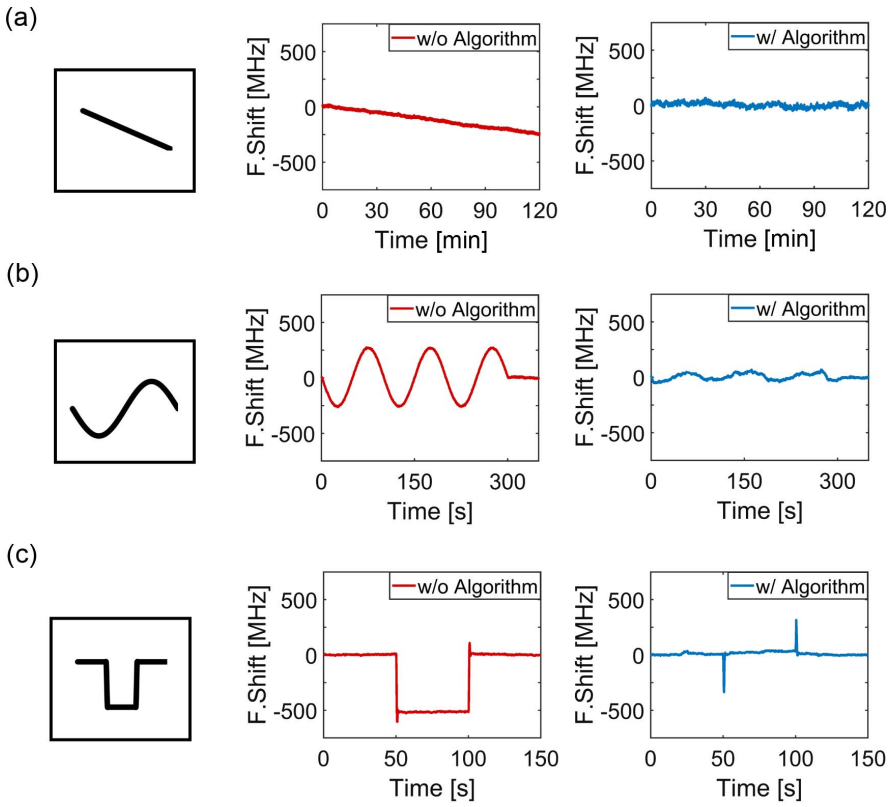

Fig. 8. Results of the experiments utilized to evaluate the stability of a 50 GHz tone, generated by the separation between the frequencies of the two lasers connected to the PIC, when the algorithm was off (red line) or on (blue line). The following thermal stimulus was applied to one of the lasers: (a) −125 MHz/hour ramp over a period of 2 hours; (b) co-sinusoidal stimulus with 100 s period and 500 MHz peak-to-peak amplitude; (c) 50 s square-like wave with −500 MHz amplitude.

capable of Tb/s communications. Future efforts will be devoted to increasing the number of stabilized lasers that the silicon nitride platform can manage and realizing a THz beat note by widely spreading two lasers from one another.

Funding. Ministero dell'Università e della Ricerca (2022H7RR4F).

Disclosures. The authors declare no conflicts of interest.

Data Availability. Data are available upon request.

REFERENCES

1. B. Isaac, B. Song, S. S. Pinna, *et al.*, "Indium phosphide photonic integrated circuit transceiver for FMCW LiDAR," IEEE J. Sel. Top. Quantum Electron. **25**, 8000107 (2019).
2. S. Arafin and L. Coldren, "Advanced InP photonic integrated circuits for communication and sensing," IEEE J. Sel. Top. Quantum Electron. **24**, 6100612 (2018).
3. R. Yan, S. P. Mestas, G. Yuan, *et al.*, "Label-free silicon photonic biosensor system with integrated detector array," Lab Chip **9**, 2163–2168 (2009).
4. R. Wang, A. Vasiliev, M. Muneeb, *et al.*, "III–V-on-silicon photonic integrated circuits for spectroscopic sensing in the 2–4 μm wavelength range," Sensors **17**, 1788 (2017).
5. H. Zhao, S. Clemmen, A. Raza, *et al.*, "Stimulated Raman spectroscopy of analytes evanescently probed by a silicon nitride photonic integrated waveguide," Opt. Lett. **43**, 1403–1406 (2018).
6. R. Nagarajan, C. Joyner, R. Schneider, *et al.*, "Large-scale photonic integrated circuits," IEEE J. Sel. Top. Quantum Electron. **11**, 50–65 (2005).
7. M. Heck, J. Bauters, M. Davenport, *et al.*, "Hybrid silicon photonic integrated circuit technology," IEEE J. Sel. Top. Quantum Electron. **19**, 6100117 (2012).
8. A. Gowen, C. O'Sullivan, and C. O'Donnell, "Terahertz time domain spectroscopy and imaging: emerging techniques for food process monitoring and quality control," Trends Food Sci. Technol. **25**, 40–46 (2012).
9. M. Karaliūnas, K. E. Nasser, A. Urbanowicz, *et al.*, "Non-destructive inspection of food and technical oils by terahertz spectroscopy," Sci. Rep. **8**, 18025 (2018).
10. M. Seo and H. Park, "Terahertz biochemical molecule-specific sensors," Adv. Opt. Mater. **8**, 1900662 (2020).
11. P. Haring Bolívar, M. Nagel, F. Richter, *et al.*, "Label–free THz sensing of genetic sequences: towards 'THz biochips'," Philos. Trans. R. Soc. London A **362**, 323–335 (2004).
12. T. Uehara, K. Tsuji, K. Hagiwara, *et al.*, "Optical beat-note frequency stabilization between two lasers using a radio frequency interferometer in the gigahertz frequency band," Opt. Eng. **53**, 124109 (2014).
13. F. van Dijk, G. Kervella, M. Lamponi, *et al.*, "Integrated InP heterodyne millimeter wave transmitter," IEEE Photon. Technol. Lett. **26**, 965–968 (2014).
14. M. Alouini, M. Brunel, F. Bretenaker, *et al.*, "Dual tunable wavelength Er,Yb:glass laser for terahertz beat frequency generation," IEEE Photon. Technol. Lett. **10**, 1554–1556 (1998).
15. R. Guzmán, L. González, A. Zarzuelo, *et al.*, "Widely tunable RF signal generation using an InP/Si_3N_4 hybrid integrated dual-wavelength optical heterodyne source," J. Lightwave Technol. **39**, 7664–7671 (2021).
16. D. A. B. Miller, "Perfect optics with imperfect components," Optica **2**, 747–750 (2015).

17. D. Coenen, H. Oprins, P. D. Heyn, *et al.*, "Analysis of thermal crosstalk in photonic integrated circuit using dynamic compact models," IEEE Trans. Compon. Packag. Manuf. Technol. **12**, 1350–1357 (2022).
18. K. Sato and M. Murakami, "Experimental investigation of thermal crosstalk in a distributed feedback laser array," IEEE Photon. Technol. Lett. **3**, 501–503 (1991).
19. I. Mathews, A. Abdullaev, S. Lei, *et al.*, "Reducing thermal crosstalk in ten-channel tunable slotted-laser arrays," Opt. Express **23**, 23380–23393 (2015).
20. D. Pérez-López, A. López, P. DasMahapatra, *et al.*, "Multipurpose self-configuration of programmable photonic circuits," Nat. Commun. **11**, 6359 (2020).
21. C. Taballione, R. van der Meer, H. Snijders, *et al.*, "A universal fully reconfigurable 12-mode quantum photonic processor," Mater. Quantum Technol. **1**, 035002 (2021).
22. C. Huang, S. Bilodea, T. F. de Lima, *et al.*, "Demonstration of scalable microring weight bank control for large-scale photonic integrated circuits," APL Photon. **5**, 040803 (2020).
23. M. Fernandez-Getino Garcia, O. Edfors, and J. Paez-Borrallo, "Frequency offset correction for coherent OFDM in wireless systems," IEEE Trans. Consumer Electron. **47**, 187–193 (2001).
24. Z. Zhang, W. Jiang, H. Zhou, *et al.*, "High accuracy frequency offset correction with adjustable acquisition range in OFDM systems," IEEE Trans. Wireless Commun. **4**, 228–237 (2005).
25. S. De, R. Das, R. Varshney, *et al.*, "Design and simulation of thermo-optic phase shifters with low thermal crosstalk for dense photonic integration," IEEE Access **8**, 141632 (2020).
26. G. Gilardi, W. Yao, H. R. Haghighi, *et al.*, "Deep trenches for thermal crosstalk reduction in InP-based photonic integrated circuits," J. Lightwave Technol. **32**, 4864–4870 (2014).
27. M. Jacques, A. Samani, E. El-Fiky, *et al.*, "Optimization of thermo-optic phase-shifter design and mitigation of thermal crosstalk on the SOI platform," Opt. Express **27**, 10456–10471 (2019).
28. X. Wu, W. Liu, Z. Yuan, *et al.*, "Low power consumption VOA array with air trenches and curved waveguide," IEEE Photon. J. **10**, 7201308 (2018).
29. M. Milanizadeh, D. Aguiar, A. Melloni, *et al.*, "Canceling thermal cross-talk effects in photonic integrated circuits," J. Lightwave Technol. **37**, 1325–1332 (2019).
30. X. Xu, G. Ren, T. Feleppa, *et al.*, "Self-calibrating programmable photonic integrated circuits," Nat. Photonics **16**, 595–602 (2022).
31. J. Ling, J. Staffa, H. Wang, *et al.*, "Self-injection locked frequency conversion laser," Laser Photon. Rev. **17**, 2200663 (2023).
32. K. Balakier, M. J. Fice, L. Ponnampalam, *et al.*, "Monolithically integrated optical phase lock loop for microwave photonics," J. Lightwave Technol. **32**, 3893–3900 (2014).
33. S. Chen and C. Chow, "Color-shift keying and code-division multiple-access transmission for RGB-LED visible light communications using mobile phone camera," IEEE Photon. J. **6**, 7904106 (2014).
34. H. Cai and A. W. Poon, "Optical manipulation and transport of microparticles on silicon nitride microring-resonator-based add–drop devices," Opt. Lett. **35**, 2855–2857 (2010).
35. H. Qiu, F. Zhou, J. Qie, *et al.*, "A continuously tunable sub-gigahertz microwave photonic bandpass filter based on an ultra-high-*Q* silicon microring resonator," J. Lightwave Technol. **36**, 4312–4318 (2018).
36. Y. Hong, Y. Hong, J. Hong, *et al.*, "Dispersion optimization of silicon nitride waveguides for efficient four-wave mixing," Photonics **8**, 16 (2021).